Macromolecules

ARTICLE

pubs.acs.org/Macromolecules

Normally Oriented Cylindrical Nanostructures in Amphiphilic PEO−LC Diblock Copolymers Films

Sadayuki Asaoka,[*,†,‡] Takayuki Uekusa,[‡] Hitomi Tokimori,[§] Motonori Komura,[‡,§] Tomokazu Iyoda,[*,‡,§] Takeshi Yamada,[⊥] and Hirohisa Yoshida[§,⊥]

[†]Department of Biomolecular Engineering, Kyoto Institute of Technology, Matsugasaki Goshokaido-cho, Sakyo-ku, Kyoto 606-0962, Japan

[‡]Division of Integrated Molecular Engineering, Chemical Resources Laboratory, Tokyo Institute of Technology, 4259 Nagatsuta-cho, Midori-ku, Yokohama 226-8503, Japan

[§]Core Research for Evolutional Science and Technology (CREST), Japan Science and Technology Agency (JST)

[⊥]Department of Applied Chemistry, Graduate School of Engineering, Tokyo Metropolitan University, 1-1 minamiosawa, Hachioji 192-0397, Japan

Supporting Information

ABSTRACT: The amphiphilic diblock copolymers consist of poly(ethylene oxide) (PEO) and poly(methacrylate) (PMA) having azobenzenes as mesogen units in the side chain afford highly ordered phase-segregated nanostructures, in which PEO cylindrical domains are hexagonally arranged and normally oriented in PMA matrix in the thin films. The liquid crystalline ordering in the strongly segregated block copolymers plays one of the most important roles to attain such an excellent arrangement of the nanostructure, potentially leading to practical use. In order to elucidate the role of the mesogen units in the side chain of the PMA segment, a new series of amphiphilic liquid crystalline diblock copolymers were synthesized to tune molecular interaction between mesogen units in liquid crystalline segments by using azobenzene, benzylideneaniline, and stilbene as mesogen cores. All the side-chain liquid crystalline diblock copolymers exhibited smectic phase and gave hexagonally arranged cylindrical nanostructures in the bulk pellets. The block copolymers having 4-(4-butylphenylazo)phenoxy, 4-((*E*)-(4-butylphenylimino)methyl)phenoxy, or 4-((*E*)-4-butylstyryl)phenoxy groups as the mesogens units gave the highly ordered hexagonal nanocylinder structures in the thin film, while the copolymers having (*E*)-4-(4-butylbenzylideneamino)phenoxy mesogen group afforded less ordered nanostructures. The former three kinds of copolymers showed obvious hypsochromic shifts and large hypochromic effects on the UV−vis spectra of annealed film, implying the formation of the strongly H-aggregated and homeotropic alignment of mesogen moieties in the PMA matrix.

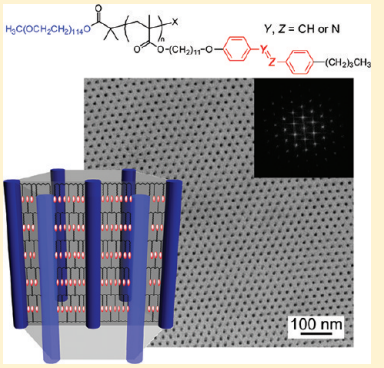

INTRODUCTION

Block copolymers composed of immiscible polymer segments form various ordered microdomain morphology in the solid state through microphase separation. The feature size of the phase separation between the polymer segments is limited to a nanometer scale because of the chemical link between the incompatible polymer components. The phase separation depends on the thermodynamic interaction parameter χ, the volume fraction of the different components, the temperature, the molecular weight, and the molecular weight distribution of the constituent component chains.[1−4] Recent remarkable progress of living polymerization methods allows one to design and synthesize various types of block polymers with well-defined structures, controlled chemical compositions, and narrow molecular weight distributions as polymer architecture.[5−13] Diblock copolymers composed of two immiscible segments have been well-known to exhibit the following ordered nanostructures in the thin films, i.e., one component of the block copolymer forms spheres arranged in a cubic face/body centered lattice, hexagonally arranged cylinders, and lamellar structure in the matrix of the other component[14] as well as more complicated but well-ordered bicontinuous morphologies.[15−18] Recently, much effort has been devoted to apply such ordered and spontaneously formed nanostructures to various fields in nanoscience and nanotechnology,[19−22] nanoporous materials,[23] nanofilters,[24−26] lithographic nanotemplates,[27−29] and electronic and/or photonic nanomaterials.[30−37] For these appreciations, it has been expected as an inevitable requirement to have uniform alignment and coaxial orientation of the phase segregated nanostructures on the macroscopic scale so as to guarantee reliable nanostructures with large anisotropy.

Liquid crystalline polymers have been extensively investigated on their unusual mechanical, optical, and rheological properties

Received: May 16, 2011
Revised: August 11, 2011
Published: September 12, 2011

Scheme 1. Preparation of Liquid Crystalline Homopolymers and Amphiphilic Diblock Copolymers via ATRP

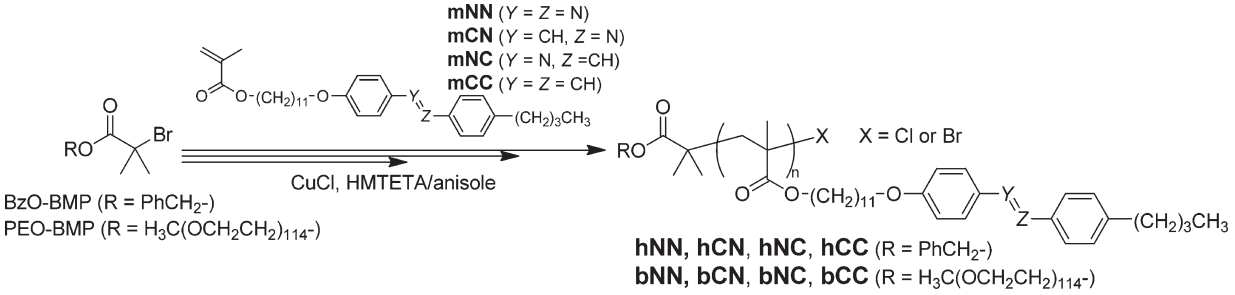

since they offer the advantageous combination of the anisotropy of liquid crystals with the attractive bulk properties of polymers.[38−42] Especially, liquid crystalline block copolymers are intriguing because of their hierarchical order, in which microphase separation of the block copolymer may occur on the 10−100 nm length scales, while liquid crystalline ordering on the length scale of the mesogen (typically 2−4 nm) appears in a certain temperature range. Since the pioneering work on the liquid crystalline block copolymer in 1985,[43] a considerable amount of effort has been devoted on the understanding of their structure/property relationships.[44] There have been several built-in methods of liquid crystallinity into block copolymers through various synthetic routes, and many different chain architectures such as segmented main-chain, rod−coil, and side-group liquid crystalline block copolymers have been reported.[45] While the synthesis of liquid crystalline main chain block copolymers with a definite structure is extremely difficult,[46−49] liquid crystalline side-group block copolymers have been easily prepared by the living polymerization techniques,[50−61] which allow us to access to the precise investigation on the correlation of two ordering principles based on the microphase segregation and liquid crystalline ordering.[62] A transmission electron microscope (TEM) and/or an atomic force microscope (AFM) observation have revealed various kinds of phase-segregated nanostructures such as sphere,[63] cylinder,[63−71] and lamellar[60,61,63,65,67,70,72−79] as well as more complicated gyroid[76] or perforated layer[80,81] structures for the liquid crystalline side-group block copolymers. It has also been reported that the liquid crystalline anisotropy and the direction of phase-segregated nanostructures in the bulk film can be simultaneously controlled by applying an electric field and/or a shear force.[66,71,81] Although the orientations of nanostructures have not been perfectly controlled yet in the thick bulk film without such external treatments to control the liquid crystalline anisotropy, De Jeu and co-workers have already demonstrated effective orientation of upright lamellar[73] or cylindrical[69] nanostructures just with thermal annealing in thin films. The extensive studies on the orientation of liquid crystalline mesogens with respect to the direction of nanostructure in the samples aligned by flow have elucidated that the relative orientation of the mesogens against the phase segregation interface depends not only on the composition of the copolymer and on the domain size[82] but also on the molecular structure of the liquid crystalline side chain.[60,61,65,67,75,76] Hammond and co-workers have synthesized a series of diblock copolymers composed of polystyrene (PS) and polymethacrylate (PMA) having smectic C* (Sm C*) liquid crystalline mesogen, which gave PS nanocylinders in the liquid crystalline PMA matrix, and concluded that the mesogens should be parallel[75] or tilted[67] to the cylinders. They have also investigated about the role of the mesogen groups by changing the fraction of liquid crystalline side chains on the poly(siloxane) segment in the PS−poly(siloxane) diblock copolymer.[83]

We have designed a new series of liquid crystalline diblock copolymers by introducing strong segregation as amphiphilicity and functionality in liquid crystalline (LC) mesogen. The amphiphilic LC diblock copolymers consists of poly(ethylene oxide) (PEO) and poly(methacrylate) (PMA) bearing azobenzene−mesogen moieties in the side chain, which gave hexagonally arranged PEO cylindrical microdomains through microphase separation in appropriate thermal annealing.[84] Emphasis should be placed on the orientation of the hexagonal PEO cylindrical nanostructures in thin film, quite different from conventional and previously reported block copolymers. The PEO cylindrical microdomains in a thin film are oriented perpendicular to the film surface on *various substrates such as silicon wafer, mica, glasses, and poly(ethylene terephthalate) film, without any surface treatment of the substrate surface*, like precoating of the corresponding random copolymer so as to adjust surface energy. Another noticeable feature is that the normally oriented and hexagonally arranged PEO cylindrical microdomains span between both the film surfaces up to several micrometers of the film thickness, i.e., >400 of aspect ratio of the PEO cylinder, which was directly confirmed by newly developed cross-sectional AFM imaging.[85] We have also succeeded in fabricating such nanostructure in a meter scale by roll-to-roll-type continuous coating. We have also demonstrated several applications of the normally oriented nanostructures: anisotropic lithium-ion conductive membranes,[26] permeable membranes with visualized high-density straight channels for small molecules,[86] addressable template thin films for periodicity- and diameter-defined arrangement of gold or silver nanoparticles,[34,87] smart BC mask with molecule-transport channels for total wet nanopatterning,[88−90] mesoporous silica nanopillar array by template sol−gel reaction,[91] and selective doping of lead ions into PEO cylindrical microdomains.[92]

We have also succeeded in controlling unidirectional arrangement of cylindrical domains by the surface rubbing of substrate,[93] which strongly implies that the liquid crystalline arrangement should play an important role to determine the cylinder orientation in thin film. Recently, Russell et al. have also demonstrated the laterally ordered cylindrical nanostructure and alignment of nanocylinders along with a topologically patterned substrate by using a block copolymer composed of PEO and polymethacrylate having 4′-cyanoazobenzene as a mesogen.[79] Hence, the combination of strong segregation system and azobenzene liquid crystalline anisotropy should play a key role to obtain such a highly ordered cylindrical nanostructure, and furthermore, such a small change in the mesogen structure could affect the direction

Table 1. Reaction Conditions of ATRP[a] and Properties of Homopolymers and Diblock Copolymers

sample	$[M]_0/[I]_0$[b]	temp (°C)	time (h)	conv[c] (%)	M_N[d]	M_W/M_N[d]	DP[e]	LC content[f] (%)
hNN$_{24}$	23	80	22	67	11 400	1.16	24	100
hNN$_{57}$	68	80	22	73	19 300	1.15	57	100
hCN$_{28}$	23	80	23	65	10 100	1.17	28	100
hCN$_{69}$	68	80	23	55	17 900	1.16	69	100
hNC$_{30}$	23	80	23	63	11 600	1.19	30	100
hNC$_{69}$	68	80	23	43	17 400	1.31	69	100
hCC$_{13}$	23	90	44	44	7 440	1.22	13	100
hCC$_{31}$	68	90	44	45	14 200	1.26	31	100
bNN$_4$[g]	10	80	22	77	9 990	1.07	4	27
bNN$_{28}$	30	80	22	70	19 300	1.13	28	73
bNN$_{56}$	60	80	22	71	25 000	1.17	56	84
bNN$_{74}$	90	80	22	64	30 300	1.20	74	88
bNN$_{104}$	120	80	22	48	37 200	1.22	104	91
bCN$_{11}$	10	80	22	34	13 500	1.10	11	51
bCN$_{30}$	30	80	22	69	19 100	1.12	30	74
bCN$_{53}$	60	80	22	66	24 700	1.16	53	83
bCN$_{73}$	90	80	22	72	30 500	1.20	73	87
bCN$_{108}$	120	80	22	61	38 100	1.21	108	91
bNC$_{10}$	10	80	23	75	14 500	1.17	10	49
bNC$_{38}$	30	80	23	76	19 500	1.25	38	78
bNC$_{63}$	60	80	23	70	24 400	1.24	63	86
bNC$_{94}$	90	80	23	70	33 200	1.29	94	90
bNC$_{120}$	120	80	23	52	40 300	1.36	120	92
bCC$_4$[g]	10	90	45	32	11 300	1.10	4	27
bCC$_{26}$	30	90	44	51	17 400	1.15	26	71
bCC$_{45}$	60	90	44	51	21 100	1.18	45	81
bCC$_{74}$	90	90	44	50	27 200	1.21	74	87

[a] $[M]_0$ = 0.2 M, polymerized in anisole under an Ar atmosphere with [BzO-BMP]/[CuCl]/[HMTETA] = 1/7.6/8.4 and [PEO-BMP]/[CuCl]/[HMTETA] = 1/10/11 for homopolymers and copolymers, respectively. [b] Fed molar ratio of monomer $[M]_0$ to initiator $[I]_0$. [c] Conversions determined by ^{1}H NMR spectra. [d] Number-averaged molecular weight and polydispersity determined by GPC analysis based on the polystylene standards. [e] Polymerization degree calculated from ^{1}H NMR spectra. [f] Weight fraction of hydrophobic poly(methacrylate) bearing LC based on DPs. [g] Purified with preparative GPC.

of nanostructure arrangement. In this paper, we wish to report syntheses, thermal property, and microphase-separated nanostructures of a series of amphiphilic liquid crystalline block copolymers, which consist of poly(ethylene oxide) (PEO) and poly(methacrylate) (PMA) bearing azobenzene, benzylideneaniline, and stilbene as mesogen cores in the side chains. Structural difference of the mesogens cores is just a linkage between two benzene rings, i.e., −*N*═N−, −CH═N−, −*N*═CH−, and −CH═CH−, which sound reasonable to elucidate the role of the mesogens units on such normally oriented cylindrical nanostructures in thin film.

■ RESULTS AND DISCUSSION

Preparation of Polymers via ATRP. The atom transfer radical polymerization (ATRP) of four kinds of methacrylate monomers **mNN**, **mCN**, **mNC**, and **mCC** having different mesogens in the side chain were conducted by using BzO-BMP as an initiator to give homopolymers **hNN**s, **hCN**s, **hNC**s, and **hCC**s, respectively (Scheme 1). The homopolymers were synthesized at two different monomer/initiator ratios ($[M]_0/[I]_0$) to control their polymerization degrees (DPs). The properties of all homopolymers are summarized in Table 1. All the homopolymers showed monomodal GPC curves, and the number-averaged molecular weights (M_Ns) increased with increasing the $[M]_0/[I]_0$ ratio. Although **hNN**s and **hCN**s gave narrow polydispersities (M_W/M_N) lower than 1.17, **hNC**s and **hCC**s showed slightly wider ones up to 1.3. The monomer **mCC** has lower reactivity for ATRP to give

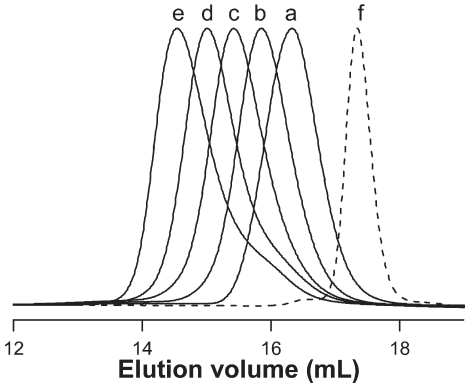

Figure 1. GPC profiles of amphiphilic diblock copolymers **bCN$_{11}$** (a), **bCN$_{30}$** (b), **bCN$_{53}$** (c), **bCN$_{73}$** (d), **bCN$_{108}$** (e), and macroinitiator PEO-BMP (f).

Table 2. Thermal Properties[a] of Poly(ethylene oxide) (PEO) and/or Liquid Crystalline Poly(methacrylate) (PMA) Blocks in Homopolymers and Diblock Copolymers

		PMA			
		transition temp (°C)		transition enthalpy (J/g)	
sample	PEO melting point (°C)	T_{SmX-Sm}	T_{Sm-I}	ΔH_{SmX-Sm}	ΔH_{Sm-I}
hNN$_{24}$		66.3	112.4	5.3	15.3
hNN$_{57}$		69.5	117.7	6.0	15.9
hCN$_{28}$		78.7	118.3	6.2	14.7
hCN$_{69}$		81.1	126.2	5.9	15.1
hNC$_{30}$		71.5	106.2	8.1	10.8
hNC$_{69}$		73.8	114.5	10.4	13.3
hCC$_{13}$		148.1	156.6	7.3	7.47
hCC$_{31}$		151.1	165.8	13.1	18.2
bNN$_{4}$	52.4	*b*	*b*	*b*	*b*
bNN$_{28}$	40.8	60.3	114.7	2.9	10.3
bNN$_{56}$	35.2	61.8	118.1	2.9	12.8
bNN$_{74}$	34.5	67.5	119.6	3.4	13.6
bNN$_{104}$	33.1	69.4	120.9	4.1	14.2
bCN$_{11}$	44.6	*b*	95.1	*b*	5.6
bCN$_{30}$	40.9	69.3	118.5	3.5	9.8
bCN$_{53}$	37.4	76.2	124.9	4.1	11.3
bCN$_{73}$	36.0	78.8	126.9	4.6	11.8
bCN$_{108}$	32.9	78.8	128.2	6.1	13.2
bNC$_{10}$	43.7	60.0	92.0	1.1	3.5
bNC$_{38}$	38.0	67.3	108.6	4.3	7.8
bNC$_{63}$	35.3	68.5	110.6	5.1	8.1
bNC$_{94}$	32.5	72.7	114.8	5.9	9.8
bNC$_{120}$	35.2	74.8	117.3	6.2	10.0
bCC$_{4}$	48.8	*b*	133.2	*b*	8.1
bCC$_{26}$	41.7	135.5	152.8	7.1	11.2
bCC$_{45}$	39.2	143.3	166.1	8.2	13.7
bCC$_{74}$	35.4	147.3	169.8	9.3	15.1

[a] Transition temperatures and enthalpies on second heating process at 10 °C/min. [b] Not determined since the transition peak was broadened and obscured.

polymers with low M_N than the other monomers at the same $[M]_0/[I]_0$ ratio, in spite of higher polymerization temperature of 90 °C and longer reaction time of 44 h. Judging from the fact that the homopolymers **hCC**s were partly precipitated on cooling the reaction mixture after polymerization, **hCC**s have a tendency to be aggregated to each other to hinder the growing site at the polymer end even at the reaction temperature.

The amphiphilic diblock copolymers **bNN**s, **bCN**s, **bNC**s, and **bCC**s were also synthesized via ATRP of the corresponding monomers using PEO-BMP as a macroinitiator at various monomer/initiator ratios in the range of 10−120 to control the DPs. The properties of all block copolymers are also summarized in Table 1. A typical set of GPC profiles for **bCN**s are shown in Figure 1. No residual macroinitiator PEO-BMP was detected in the GPC profiles after polymerization, suggesting that the PEO-BMP quantitatively initiates the polymerization irrelevant to the mesogen structure in the side chain. Monomodal GPC curves were obtained, and the M_Ns were simply increased with increasing the $[M]_0/[I]_0$ ratio for all copolymers. The ATRP of monomer **mCC** gave lower M_Ns than that of the other monomers at the similar $[M]_0/[I]_0$ ratio, and the copolymer having higher M_N than **bCC$_{74}$** could not be obtained probably because of reducing reactivity of the growing end sterically hindered by its aggregation. The polydispersities of **bNC**s were slightly higher than those of the other copolymers. The imino groups in the mesogen core of monomers **mCN** and **mNC** are Schiff base, and the basicity of **mCN** should be stronger than that of monomer **mNC**.[94] The ^{1}H NMR spectra of **mCN** and **mNC** were measured in the presence of excess CuCl in the mixed solvent of CD_3OD and $CDCl_3$ (5:1). The peaks for imino proton were broaden and shifted by 0.17 and 0.098 ppm for **mCN** and **mNC**, respectively, the tendency of which was in accordance with their basicity. However, little peak shifts were observed by adding equimolar HMTETA. This fact implies that the formation of imino−copper complex itself might not disturb the catalytic cycle of ATRP in the actual reaction mixture. The color of the ^{1}H NMR sample solution containing monomer **mNC** and CuCl was gradually changed to brown while such a change was not observed for monomer **mCN**. Although any obvious new peaks could not be detected on the ^{1}H NMR spectrum of **mNC**, some undesired decomposition of monomer or a charge transfer in the imino−copper complex should have occurred, which would have a bad influence on ATRP. Although little change in the ^{1}H NMR spectrum of **mNC** was detected, some undesired decomposition of monomer or a charge transfer in the imino−copper complex could occur, which would have a considerable influence on ATRP.

Liquid Crystalline Properties of Homopolymers. Thermal properties of the polymers were investigated by using differential scanning calorimetry (DSC), and their liquid crystalline phases were assigned on the basis of the polarized optical microscopic (POM) textures and the wide-angle X-ray diffraction (WAXD) patterns.

While the monomers **mNN**, **mCN**, **mNC**, and **mCC** gave a set of melting and crystallization peaks upon heating and cooling processes in the DSC profiles and indicated no liquid crystalline character, all the homopolymers **hNN**s, **hCN**s, **hNC**s, and **hCC**s obviously showed liquid crystalline transitions in DSC curves, judging from POM textures and WAXD patterns. The transition temperatures together with the corresponding transition enthalpies are summarized in Table 2. Typical DSC curves on the first cooling and second heating processes are shown in Figure 2. The homopolymer **hNN$_{57}$** showed two well-defined endothermic transitions at 70 and 118 °C together with a very small transition around 109 °C on heating, and their corresponding exothermic transitions were observed on cooling with a few degree of supercooling effect. POM observation of **hNN$_{57}$** was conducted under control of the sample temperature with a Mettler FP-82 hot stage. Once **hNN$_{57}$** was heated to 140 °C, just black-out views with no texture were observed at the cross Nicole optical setting, suggesting an isotropic phase. As shown in the right images of Figure 2, a focal conic-fan-shaped texture, which is assigned as smectic A (SmA) phase, appeared in the temperature range 119−105 °C on cooling. A slight texture change was observed around 100 °C, which was identified as a phase transition from SmA to smectic C (SmC) phase, as reported previously.[84] On further cooling below 70 °C, the textures became obscure.

In the case of **hCN$_{69}$**, two similar transition peaks were observed at 81 and 126 °C, but any other peaks were not detected between them. On a POM observation, a slightly

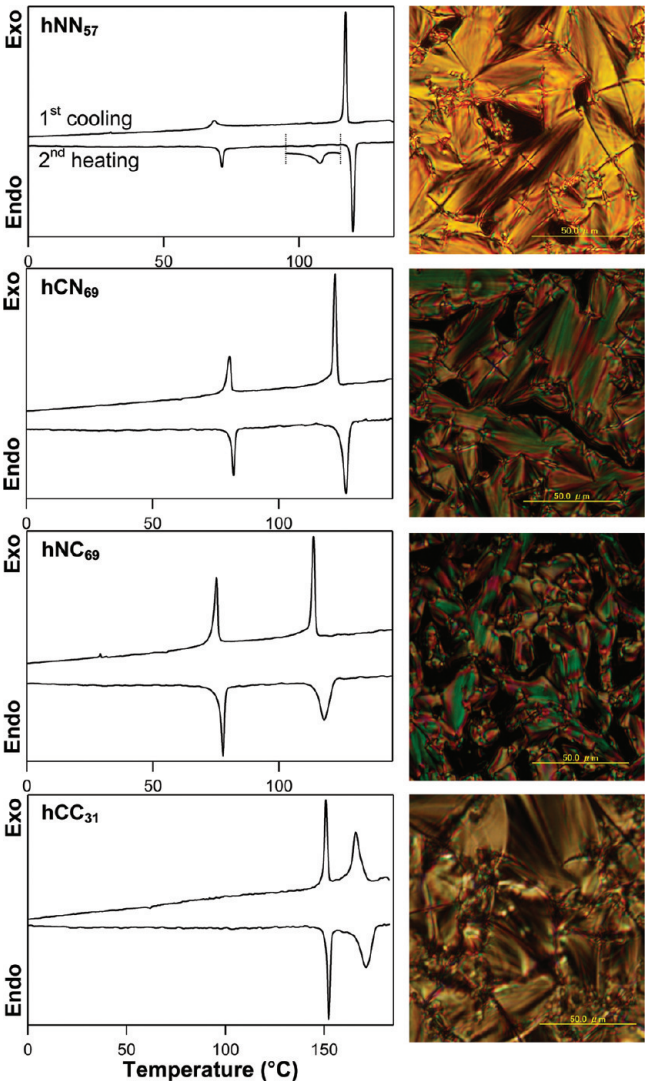

Figure 2. DSC curves of homopolymers on first cooling and second heating processes with heating/cooling rate of ±10 °C/min (left traces) together with the polarized optical micrographs around isotropic transition temperature (right images). **hNN$_{57}$** at 118 °C, **hCN$_{69}$** at 120 °C, **hNC$_{69}$** at 113 °C, and **hCC$_{31}$** at 160 °C.

unclear focal conic-fan-shaped texture was obtained in the temperature range 115−80 °C, as shown in Figure 2. On further cooling below 80 °C, the texture similarly became obscure. In the case of **hNC$_{69}$**, two transition peaks appeared at 74 and 115 °C, and the POM texture became more unclear than that of **hCN$_{69}$**. The liquid crystalline phase of **hNC$_{69}$** therefore could not be fully assigned here by DSC and POM. In contrast to **hNN$_{57}$**, **hCN$_{69}$**, and **hNC$_{69}$**, **hCC$_{31}$** gave two transition peaks at much higher temperatures (151 and 166 °C). A clear focal conic-fan-shaped texture was observed on POM in the temperature range 168−150 °C, indicating SmA phase. The texture also became obscure on further cooling below 150 °C. The intermediate temperature region (around 15 K) of **hCC$_{31}$** assigned as a smectic liquid crystalline phase was considerably narrower, and the transition enthalpies of two transitions for **hCC$_{31}$** were fairly larger than those of the other homopolymers.

In order to assign the liquid crystalline phase of each homopolymer, temperature-dependent WAXD measurement was

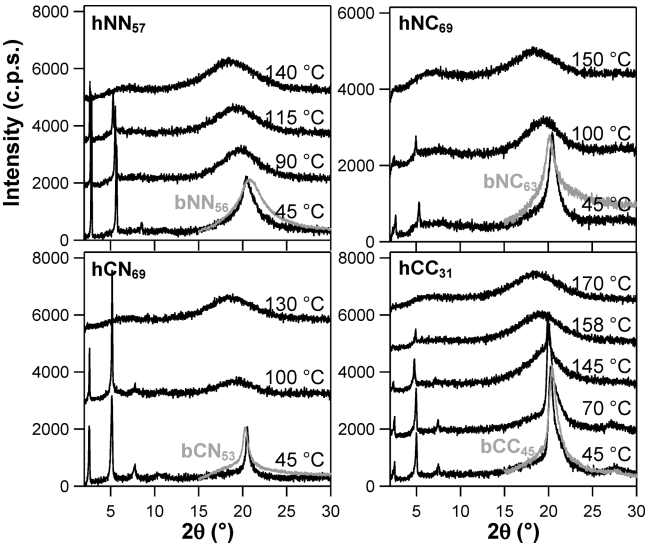

Figure 3. WAXD profiles of homopolymers (black) and amphiphilic diblock copolymers (gray lines) at representative temperatures.

conducted. The WAXD profiles at the representative temperatures are shown in Figure 3. Two or three sharp diffraction peaks were observed in a small-angle region for all polymers at the intermediate temperature range between two peaks on DSC profiles. These peaks for **hNN$_{57}$** were assigned as [001], [002], and [003] diffractions derived from the layer structure of smectic phase with the periodicity d_L of 3.34 nm at 115 °C. As we reported previously,[84] the peaks observed for **hNN$_{57}$** were shifted to a wider 2θ angle region on cooling with the layer spacing d_L of 3.11 nm at 45 °C. Since this layer spacing is smaller than the fully extended side chain length of 3.29 nm calculated by the MM2 force field method, the phase at 45 °C may be assigned to tilted smectic phase, in which the tilt angle of mesogen-containing side chains can be estimated as 23°. In the case of **hNC$_{69}$**, a set of weak peaks assigned as [001] and [002] diffractions was observed, suggesting a kind of smectic layer structure. The layer spacing was also shrunk on cooling from 3.54 at 100 °C to 3.31 nm at 45 °C, but it was almost comparable to the fully extended side chain length of 3.32 nm even at 45 °C. In contrast, the small-angle peaks for **hCN$_{69}$** and **hCC$_{31}$** shifted little to wider angle during cooling once appeared. The layer distance of **hCN$_{69}$** was almost unchanged from 3.43 nm, which is larger than the fully extended side chain lengths of 3.28 for **2**. The calculated layer spacing of **hCC$_{31}$** was once increased from 3.59 nm at 158 °C to 3.71 nm at 145 °C and then decreased again on cooling to 3.53 nm at 45 °C. We should emphasize here again that the layer distances in **hCC$_{31}$** were larger than the fully extended side chain length of 3.30 nm for **mCC** at any temperatures lower than isotropic transition temperature. Summarizing the results from the thermal properties, the liquid crystalline textures, and the layer structures for the homopolymers obtained above, we can assign the liquid crystalline phases of **hCN$_{69}$** and **hCC$_{31}$** as SmAs.

A relatively broad peak was also observed for all the homopolymers at around 20°, which originated from the lateral correlation among the mesogens in the side chain. These broad peaks in liquid crystalline phase become dramatically sharper in the lower temperature region than the second transition peaks on cooling in the DSC curves at 66−81 °C for **hNN**s, **hCN**s, and

hNCs and around 150 °C for **hCC**s, implying the formation of long-range bond orientational order in the intralayer mesogen arrangements (see the Supporting Information for details).

The width of the small angle diffraction peaks reflects from the "interlayer" regularity as a persistent length of the layered structure in the smectic phase. $\mathbf{hNC_{69}}$ gave a set of weak and relatively wide diffraction peaks while the other homopolymers showed sharp and intense peaks up to third diffraction. Although the accurate estimation of the interlayer regularity (D_Ls) should be difficult because of the insufficient data points in the small angle diffraction region, the D_L values of each homopolymer was also roughly estimated to be 170 nm for $\mathbf{hNN_{57}}$, 120 nm for $\mathbf{hCN_{69}}$, 100 nm for $\mathbf{hNC_{69}}$, and 140 nm for $\mathbf{hCC_{31}}$ by applying the Scherrer equation.[95] $\mathbf{hNC_{69}}$ should have some disordering in the liquid crystalline layer structure to give a lower regularity than the other homopolymers.

Thermal Properties of Amphiphilic Diblock Copolymers. Thermal properties of diblock copolymers **bNN**s, **bCN**s, **bNC**s, and **bCC**s were also investigated. Typical DSC curves on the first cooling and second heating processes for are shown in Figure 4. Two transition peaks were also observed for all copolymers at comparable temperature to the corresponding homopolymers. The transition temperatures and transition enthalpies are also summarized in Table 2. The mesophase were also identified by POM observation. As illustrated in the right images of Figure 4, definite batonnet textures, which are typical for a SmA liquid crystalline phase, were observed at the first liquid crystalline transition peak for $\mathbf{bNN_{56}}$, $\mathbf{bCN_{53}}$, and $\mathbf{bCC_{45}}$. In the case of $\mathbf{bNC_{63}}$, dark and unclear in the figure, but still a very fine batonnet texture was observed, implying that the liquid crystalline phase of $\mathbf{bNC_{63}}$ could be assigned as a SmA, but the domain size should be considerably smaller than that of the other copolymers. On further cooling, the batonnet grew to cover all area in the microscope view and then become obscure in the temperature region below the second liquid crystalline transition. As shown in Figure 3, broader diffraction peaks on WAXD were observed for the block copolymers in a wide angle region around 20° than that of corresponding homopolymers, implying that the growth of the quasi-crystalline region in the intralayer direction should be restricted by the regularly arranged cylindrical domains with 17−18 nm of distances between them (see the Supporting Information for details).

In addition to the liquid crystalline transition peaks, another set of peaks were observed for all samples in the lower temperature region than 50 °C. A definite peak at around 35 °C was observed for each copolymer on heating, which is assigned as a melting point of PEO segment. On cooling, the corresponding freezing points were getting down to the temperature region below −10 °C by overcooling effect. Typical DSC curves for a series of copolymers **bCN**s with different polymerization degrees are given in Figure 5. On heating, while the two peaks based on liquid crystalline phase transitions became obscured and were shifted to lower temperature with the polymerization degree of PMA segment decreasing, the melting point of PEO segment were shifted to higher temperature and getting closer to that of PEO-BMP macroinitiator. In contrast, the freezing point showed discontinuous change; the copolymers having short PMA segment with less than 30 monomer units gave a freezing point at around 20−30 °C, and the other copolymers having longer hydrophobic segment with more than 50 monomer units were suffered from the considerable overcooling effect to give a freezing point below −10 °C. In the case of $\mathbf{bCC_{45}}$, two

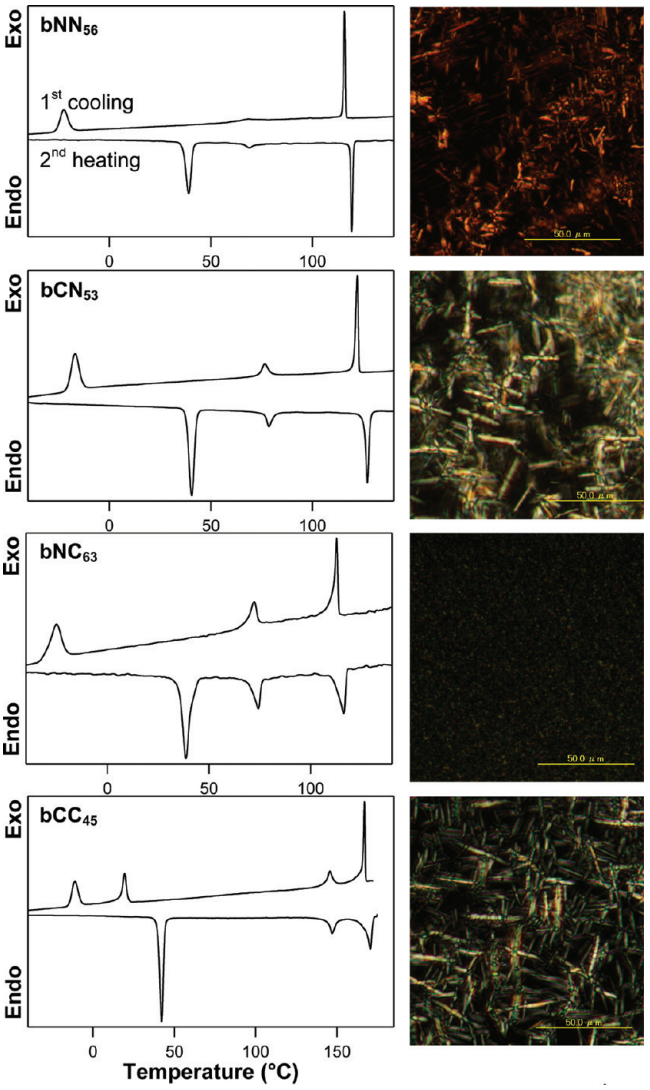

Figure 4. DSC curves of amphiphilic diblock copolymers on first cooling and second heating processes with heating/cooling rate of ±10 °C/min (left traces) together with the polarized optical micrographs around isotropic transition temperature (right images). $\mathbf{bNN_{56}}$ at 118 °C, $\mathbf{bCN_{53}}$ at 126 °C, $\mathbf{bNC_{63}}$ at 115 °C, and $\mathbf{bCC_{45}}$ at 168 °C.

transition peaks attributable to the freezing of PEO segment were observed in both temperature areas, simultaneously. On cooling at the freezing point, the PMA segment is immobilized in the hexatic phase, and the mobility of PEO chain should be therefore restricted to hinder the crystallization of PEO segment, called a confined effect. As a result, the freezing point was considerably lowered, and the crystal structure of PEO might be also disordered, especially at the interface to PMA segment, to afford a melting point at lower temperature upon heating compared to PEO-BMP and to the copolymers having shorter PMA segment. Although the mechanism for the discontinuous behavior of freezing point in changing the polymer length have not fully elucidated by now, the crystal structure of PEO might be changed according to the length of PMA segment at the polymerization degree of around 40.

According to Table 2, the transition temperatures and enthalpies attributable to liquid crystalline transitions were increased with increasing PMA fractions for all series of block copolymers. The

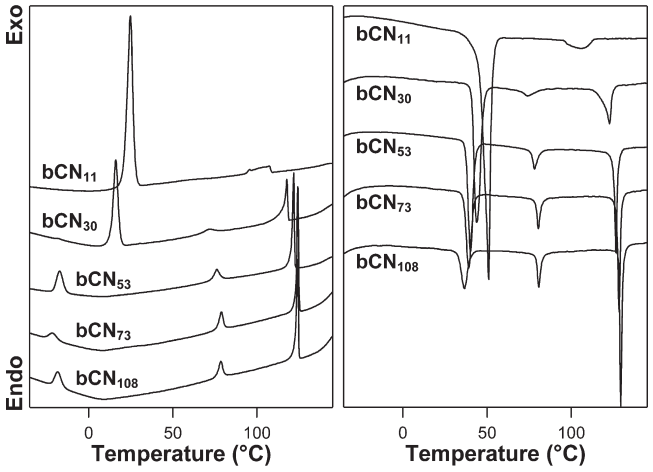

Figure 5. DSC curves of amphiphilic diblock copolymers **bCN**s on first cooling (left) and second heating (right) processes with heating/cooling rate of ±10 °C/min.

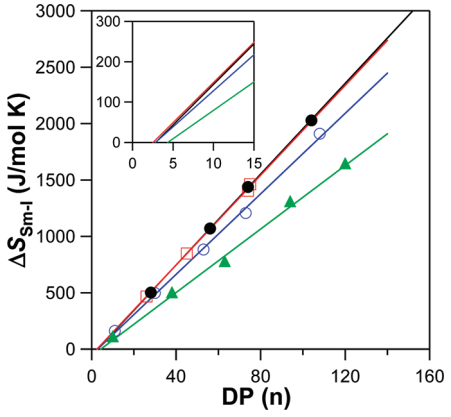

Figure 6. Relationship between differential transition entropies for isotropic transition (ΔS_{Sm-I}) and polymerization degrees of PMA segment (DPs) in amphiphilic diblock copolymers. Inset gives an enlarged plot for low DP region. **bNN**s (black closed circle), **bCN**s (blue open circle), **bNC**s (green closed triangle), and **bCC**s (red open square).

transition entropies calculated from the enthalpies are useful to analyze the effect of mesogen structures upon liquid crystalline ordering. The differential entropies for the isotropic transitions ΔS_{Sm-I} were calculated by the following equation

$$\Delta S_{Sm-I} = \Delta H_{Sm-I}/T_{Sm-I}$$

where ΔH_{Sm-I} and T_{Sm-I} represent the transition entropy and temperature for isotropic transition, respectively. Assuming that the total entropies in an isotropic state are equal for all copolymers, ΔS_{Sm-I} should represent the orderness of the smectic phase just after the phase transition. In Figure 6, the differential entropies ΔS_{Sm-I} were plotted against the averaged polymerization degrees (DP) of copolymers, which gave a linear relationship for each copolymers. The fact that extrapolated lines of all the plots give almost same x-intercepts of DP = 3−4, implying that not more than four liquid crystalline monomer units are disordered at the microphase interface. Thus, all copolymers should be in a strong segregation system to form very sharp and contrastive interfaces between PEO and PMA domains. In addition, the increment of each plot represents an entropy gain by arranging one liquid crystalline unit (monomer unit) to the ordered SmA layer structure, reflecting the extent of ordering of a SmA structure formed at the temperature region adjacent to the SmA−I phase transition. The increments of the plots for the series of **bNN**s and **bCC**s were almost comparable, and larger than that of **bCN**s and **bNC**s, suggesting that copolymers **bNN**s and **bCC**s have well-ordered liquid crystalline structure more than the other copolymers. The copolymer **bNC**s, having a smallest increment as much as 70% of that of **bNN**s and **bCC**s, should have most disordered liquid crystalline alignment and, as a result, gave relatively broad transition peaks on DSC as well as unclear textures on POM observation compared with other series of polymers. Since the tacticity cannot be controlled under ordinal ATRP conditions, the PMA main chain should be atactic, and therefore the side chains are placed randomly at either side of the backbone and interdigitated between the smectic layers. Judging from the molecular structure, the benzylideneaniline mesogens in monomer unit **mCN** or **mNC** have a large dipole moment compared to both mesogens in **mNN** and **mCC**. An antiparallel arrangement of mesogens should be formed in the array of interdigitated side chains, which is more unfavorable for the azomethyne mesogens in **bCN**s and **bNC**s than the others to disturb the arrangement of stacked mesogens.

Nanostructures in Bulk Sample. The amphiphilic diblock copolymers afforded phase-segregated nanostructure through annealing at the higher temperatures than the isotropic phase transition temperatures. In order to identify the nanostructure, SAXS measurement of the bulk pellet of copolymers were conducted. The sample pellets of **bNN**s, **bCN**s, and **bNC**s were annealed under vacuum at 140 °C, and the annealing temperature was changed to 190 °C in the case of **bCC**s. Typical SAXS profiles of are shown in Figure 7a. Two peaks observed at low scattering vector (q) range below 0.9 nm^{-1} were assigned as the diffraction from (100) and (110) planes of hexagonally ordered cylindrical structure, where $(d_{110})^{-1} = \sqrt{3} \times (d_{100})^{-1}$. The third peak based on the diffraction from the (200) plane was also observed at the position of $(d_{200})^{-1} = \sqrt{4} \times (d_{100})^{-1}$ as a shoulder peak of the second peak. Although the peak patterns for **bNN**$_4$ and **bCC**$_4$ having very short PMA segments were not matched to these hexagonally arranged nanostructure, it can be concluded that the other copolymers show the hexagonally ordered cylindrical nanostructure as a common microphase-separated structure by using the AFM study, as will be discussed later. The distances between (100) planes (d_{100}) calculated from the scattering vectors of first peak for all copolymers are plotted against the polymerization degree of PMA in Figure 8. The d_{100} values were increased with the increase of DPs. The DP range of the block copolymers is too narrow for us to quantitatively discuss the relationship between the d_{100} and DP, but it should be added that such scattered data are within the welknown power rule of 2/3. There are no obvious difference based on mesogen structure, suggesting that the distance between (or periodicity of) hexagonally ordered cylinders is determined only by the volume fraction of PMA segment irrelevant to the mesogen structure.

Temperature-dependent SAXS profiles for **bNN**$_{56}$, **bCN**$_{73}$, **bNC**$_{63}$, and **bCC**$_{45}$ are illustrated in Figure 7b. Intense first and second diffraction peaks were observed in the temperature range where PEO segment is crystallized. The intensities of the peaks were decreased, but the hexagonal structure still remained at higher temperature than the melting point of PEO. In the temperature range above isotropic transition, these diffraction

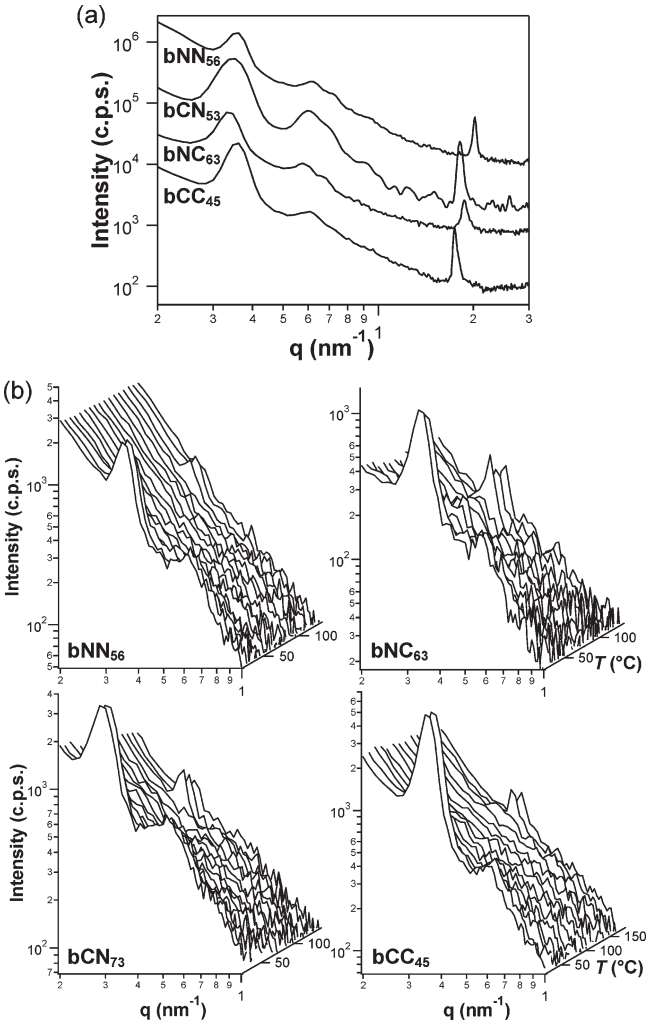

Figure 7. SAXS profiles for amphiphilic diblock copolymers. (a) SAXS profiles at ambient temperature for the bulk pellets of block copolymers annealed at higher temperature than the corresponding T_{Sm-I}. **bNN$_{56}$**, **bCN$_{53}$**, and **bNC$_{63}$** were annealed at 140 °C, and **bCC$_{45}$** was annealed at 190 °C. (b) Stacked SAXS profiles for **bNN$_{56}$**, **bCN$_{73}$**, **bNC$_{63}$**, and **bCC$_{45}$** given by temperature-dependent measurement.

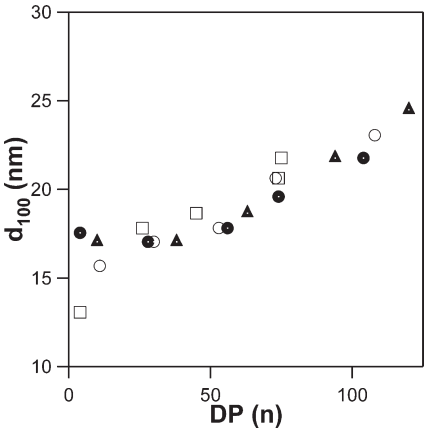

Figure 8. Layer spacing of (100) plane calculated from the scattering vector of the first peak in SAXS profile plotted as a function of DPs. **bNN**s (closed circle), **bCN**s (open circle), **bNC**s (closed triangle), and **bCC**s (open square).

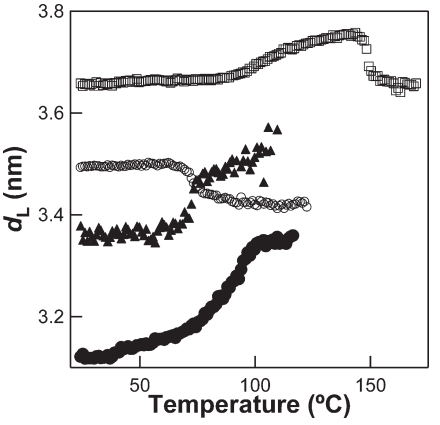

Figure 9. Smectic layer distances estimated by scattering vectors in temperature-dependent SAXS profiles. **bNN**s (closed circle), **bCN**s (open circle), **bNC**s (closed triangle), and **bCC**s (open square).

peaks become intense again. Similar behavior was also observed for the other series of copolymers. While the position of the first diffraction peak was almost not shifted in the case of the copolymers having relatively longer PMA segment in the temperature range above the isotropic transition, it was slightly changed and/or obscured in the typical case of some copolymers with short PMA segment, suggesting that a hexagonal-to-body centered cubic phase transition or other order-to-order transition would occur simultaneously with the isotropic transition of liquid crystalline phase. The hexagonally arranged phase-segregated nanostructure has already been formed in the temperature range around isotropic transition and preserved down to room temperature.[96]

The peaks around 2 nm^{-1} are due to the diffraction from the smectic layer structure. The smectic layer distances at room temperature were calculated to be 3.12 nm for **bNN**s, 3.50 nm for **bCN**s, 3.35 nm for **bNC**s, and 3.65 nm for **bCC**s, irrelevant to the polymerization degree of PMA segment. Applying the Scherrer equation[95] to their half-width, the interlayer regularity (D_L) along the smectic layers was roughly estimated by to be 170 nm for **bNN$_{56}$**, 130 nm for **bCN$_{53}$**, 100 nm for **bNC$_{63}$**, and 190 nm for **bCC$_{45}$**, which were almost comparable to those of the corresponding homopolymers obtained above. As described above, the mismatches in the dipole moment of azomethyne mesogens might induce the disordered arrangements of the layer structure to reduce the interlayer regularity.

The diffraction peaks based on the smectic layer structure were shifted depending on temperature. The smectic layer distances (d_L) evaluated from the peak position on temperature-dependent SAXS measurements are plotted as a function of temperature in Figure 9. The layer distances around the isotropic transition temperatures for all copolymers are longer than 3.34 nm, which is the fully extended side chain length of 3.28−3.32 nm for the monomers calculated by MM2 force field method, indicating the existence of a SmA phase for all block copolymers in this temperature region. In the case of **bNN**s, the layer spacing began to shrink at 102 °C, reached the comparable length with the side chain length at 94 °C, and kept shrinking down to 3.12 nm at room temperature. The side chains together with mesogens in **bNN**s should therefore be tilted in the temperature

range below 94 °C. The slope of the plot appeared to be changed around 70 °C, where the second transition peak attributable to the smectic C-to-hexatic phase transition was observed on DSC. The layer spacing for **bNC**s was also gradually shrunk on cooling but reached the length of 3.34 nm, which is slightly longer than the side chain length, even at room temperature. This suggests that the liquid crystalline phase transition based on the layer shrinking observed for **bNN**s should not occur in the case of **bNC**s. While the layer spacing of **bNN**s was gradually shrunk on cooling, that of **bNC**s was dramatically changed around 72 °C, of which temperature agrees with the second liquid crystalline transition temperature of **bNC**s.

In contrast, the layer distance of **bCN**s was gradually expanded on cooling and changed dramatically around their second transition temperature. The layer spacing is longer than the side chain length at any temperatures below the isotropic transition, and thus the liquid crystalline phase should be unchanged from the SmA phase. In the case of **bCC**s, the layer distance was immediately expanded at the temperature of 149 °C, which exactly coincides with the second transition temperature observed on DSC and gradually shrunk to comparable layer distance with initial one at room temperature. Here, the layer spacing was considerably larger than the side chain length by 0.35−0.45 nm, and **bCC**s should therefore exhibit SmA phase at any temperature below the isotropic transition temperature. The slope of plot was changed to almost flat at 90 °C, which would result from the glass transition of PMA main chain, judging from the fact that the glass transition temperature of atactic poly(methyl methacrylate) (PMMA) is known to be around 70 °C. The hexatic phase transitions and the glass transitions of PMA main chain for **bNN**s, **bCN**s, and **bNC**s should exist in the same temperature area and therefore could not be observed separately.

Nanostructures in Thin Film. The thin films of the amphiphilic diblock copolymers were prepared by spin-coating from their toluene or chloroform solutions on the mica or Si wafer substrates. The film thickness can be controlled over the several hundred nanometers region by changing the sample concentration and/or the spinning rate upon coating. Much thicker films up to 2 μm of thickness can be prepared by bar-coating.

The nanostructures in the thin films of less than 200 nm thickness can be imaged by TEM observation. The samples for **bNN**s, **bCN**s, and **bNC**s were annealed under vacuum at 140 °C for 24 h while that for **bCC**s at 190 °C for 2 h. Typical TEM images are shown in the left images of Figure 10. While the nanostructures with obvious regularity could not observed for the thin film of $\mathbf{bNN_4}$ and $\mathbf{bCC_4}$, the PEO domains selectively stained by RuO_4 exhibit as hexagonally arranged dots with a diameter about 3 nm dispersed into the unstained PMA matrix in the case of **bNN**s, **bCN**s, and **bCC**s. The periodicities of dots well agreed with that calculated from the scattering vectors of first peak in SAXS profiles. In the fast Fourier transformation (FFT) profile of each TEM image, at least third-order peaks were observed, suggesting that the dots are well arranged in a hexagonal manner. In contrast, TEM image of **bNC**s gave a less ordered dot pattern, while the SAXS indicated a hexagonally arranged structure. The FFT image of **bNC**s gave a ring pattern, suggesting that interdot distance seems constant but little orderness is found in their arrangement.

Typical phase-shift images of the film surface obtained by AFM observation are given in the right images of Figure 10. The hexagonally arranged dot patterns were observed over the whole surface. The dots and their surrounding matrices are assigned to

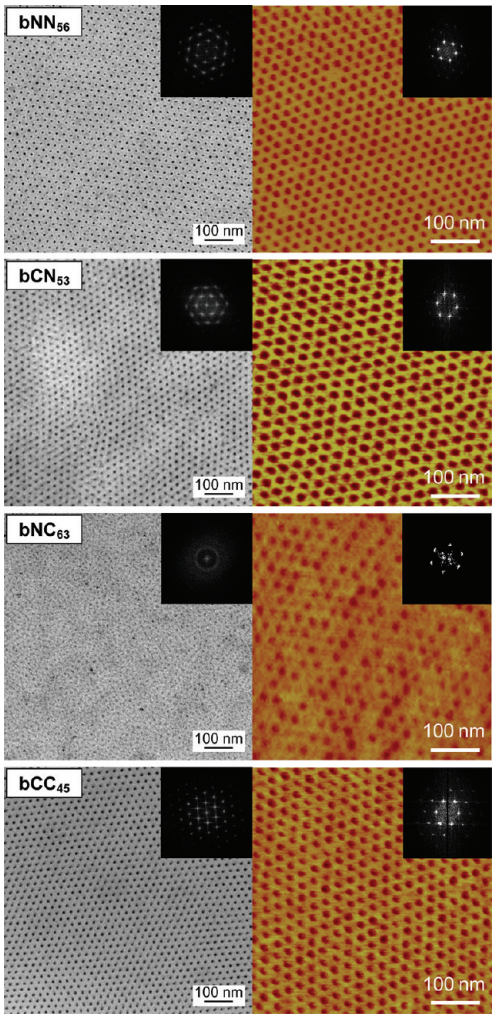

Figure 10. TEM images of amphiphilic diblock copolymer thin films (left images) and AFM phase-shift image of surfaces of their bar-coated films (right images). Insets are 2D Fourier-transformed images.

the PEO cylindrical and the PMA matrix domains, respectively, judging from their viscoelastic property. The similar highly ordered dot patterns were observed for the block copolymer $\mathbf{bNN_{56}}$, $\mathbf{bCN_{53}}$, and $\mathbf{bCC_{45}}$ films over the range of 100 nm to 2 μm thickness, implying that the hexagonal PEO cylindrical domains are oriented perpendicularly in the $\mathbf{bNN_{56}}$, $\mathbf{bCN_{53}}$, and $\mathbf{bCC_{45}}$ thin films. The well-arranged dot patterns in the AFM images correspond to the (001) face of the perpendicularly oriented hexagonal cylinder structure in thin films. Even $\mathbf{bNC_{63}}$ gives a well-ordered dot pattern as the (001) face of the hexagonal cylinder nanostructure in the AFM image and especially a clearly observed hexagonal FFT pattern of the image, although the TEM image illustrated a less ordered nanostructure than the other block copolymers. These images indicate that $\mathbf{bNC_{63}}$ should have a shot-range ordering in its nanostructure as hexagonal cylinder phase but could give a multidomain structure consisting of smaller domain size than those of the other block copolymers.

The block copolymers **bNN**s, **bCN**s, and **bCC**s gave the PEO cylindrical microdomains in a thin film oriented perpendicular to the film surface on various substrates such as silicon wafer, mica, glasses, and poly(ethylene terephthalate) films irrespective of the

surface energy of substrate. The phase transition and the growth of cylindrical nanostructure might therefore occur from the free surface of the thin film bound to air to the back surface in contact with the substrate surface. Although the liquid crystalline diblock copolymers composed of PS or poly(methyl methacrylate) (PMMA) in the place of PEO have been reported by Seki et al.[97] and Alcalá et al.,[77] these copolymers gave slightly disordered cylindrical or lamellar structure in the thin films, suggesting that the mobility of the PS or PMMA segments might be more restricted than that of PEO to disturb the growth of nanostructure because of their high glass transition temperatures. It should be therefore important for the formation of highly orderd cylindrical nanostructure to keep the polymer chain free during the mesogen arrangement.

UV−vis Spectra Change upon Nanostructure Formation. The mesogen chromophores used in this study have characteristic absorption bands in UV and near-UV regions. Independently, the following model compounds were synthesized as repeated units of the PMA segments of the amphiphilic liquid crystalline block copolymers in this study: 11-(4-((*E*)-4-butylphenylazo)-phenoxy)undecyl 2′-methylpropionate (**NN**), 11-(4-((*E*)-(4-butylphenylimino)methyl)phenoxy)undecyl 2′-methylpropionate (**CN**), 11-((*E*)-4-(4-butylbenzylideneamino)phenoxy)undecyl 2′-methylpropionate (**NC**), and 11-(4-((*E*)-4-butylstyryl)phenoxy)-undecyl 2′-methylpropionate (**CC**) as reference compounds of monomer **mNN**, **mCN**, **mNC**, and **mCC**, respectively. The left traces of Figure 11 show their UV absorption spectra in hexane. The azobenzene chromophore in **NN** has strong absorption at 237 and 346 nm having less resolved vibration structures which correspond to $\pi-\pi^*$ transitions of the *E* form, of which transition dipole moments are short and long axes of the azobenzene chromophore, respectively. A weak and broad absorption band observed around 440 nm is assigned to the $n-\pi^*$ transition of its *Z* form, which was partly formed under exposure to room light. When the solution was kept in the dark for a few days at room temperature, this absorption disappeared due to thermal isomerization from *Z* to *E* forms. The stilbene chromophore in **CC** has a short axis $\pi-\pi^*$ transition at 228 nm and vibrationally split long axis $\pi-\pi^*$ transitions at 305 and 322 nm, of which the energy difference is 1710 cm^{-1}, corresponding to C−C stretching vibration of the benzene ring. On the contrary, the benzylideneaniline chromophores in **CN** and **NC** as mesogen cores have a couple of long axis $\pi-\pi^*$ transitions at 280 and 322 nm for **CN** and 271 and 336 nm for **NC**, respectively. These splits could not result from any vibrational structure but from independent electronic transitions, since the energy differences of the paired transitions are 4610 cm^{-1} for **CN** and 7160 cm^{-1} for **NC**. Their short axis $\pi-\pi^*$ transitions are located at 280 and 322 nm for **CN** and 271 and 336 nm for **NC** with vibrational structures.

As shown in the left traces of Figure 11, two set of spectra of the chloroform solutions of the block copolymers with different concentrations are recorded: One is $(3.3-3.6) \times 10^{-5}$ mol L^{-1} per mesogen chromophore for discussion on electronic transitions of the isolated mesogen chromophores. The other is 2 wt %, which was used for the spin-coating solution and corresponds to approximately $(5.1-5.5) \times 10^{-2}$ mol L^{-1} per mesogen chromophore for the block copolymers. In diluted chloroform solution the long axis $\pi-\pi^*$ absorption bands of all four block copolymers look almost similar to those of the reference compounds in hexane solution mentioned above, except for small blue shift with a few to ten nanometers and less vibrational structures. However, long tails down to more than 1000 nm are observed in the concentrated chloroform solutions, although the absorption bands of the mesogen chromophores go off the scale. These tails can be explained by Rayleigh scattering due to polymer micelle formation, which sounds reasonable with respect to the amphiphilicity of the block copolymers used in this study. The scattering coefficient is formulated as $k \propto d^5\lambda^{-4}$, where d and λ are diameter of the scattering particle and wavelength of light, respectively. When the magnitude of the scattering is evaluated roughly as optical density in a much longer wavelength region, here in 500−800 nm, than the absorption bands of the mesogen chromophores, it can be said that the polymer micelles would form in the concentrated chloroform solution in the order of $\mathbf{bNN_{56}} > \mathbf{bNC_{63}} \geq \mathbf{bCC_{45}} \gg \mathbf{bCN_{53}}$. Such polymer micelle formation would be much more serious during solvent evaporation process in the spin-coating to give the thin films, in which the micelles would be aggregated to give close-packed micelle structures observed in the spin-coated films before annealing. Such dynamic processes should be investigated so as to understand the normally oriented hexagonal cylinder nanostructure after annealing, which is beyond this study and will be reported elsewhere.

The right traces of Figure 11 show UV absorption spectra of the spin-coated films of the block copolymers before and after annealing. These spectra were taken in 250−600 nm because of serious light scattering of the spin-coated films in a shorter wavelength region than 250 nm. The as-coated film of $\mathbf{bNN_{56}}$ gives an absorption maximum at 337 nm due to the $\pi-\pi^*$ long axis transition of the azobenzene unit, which is blue-shifted by 16 nm from that in chloroform solution. After annealing at 140 °C in the isotropic phase, $\mathbf{bNN_{56}}$ film exhibited a hypsochromic shift by 11 nm, suggesting a formation of strong H-aggregation of azobenzene chromophores in the liquid crystalline PMA matrix. The absorbance of the annealed film was decreased 62% from that of the as-cast film, which is attributable to the homeotropic alignment of the mesogen unit in the side chains to the substrate surface.[97,98] The short axis $\pi-\pi^*$ transition of the azobenzene unit looks neither hypsochromic shift nor hypochromic effect, since this transition dipole moments would be distributed randomly in plane orthogonal to incident light regardless of the homeotropic alignment of the mesogen units. As we reported previously,[84] only a slight decrease (<15%) of absorbance and no blue shift were observed upon annealing at 105 °C in the smectic liquid crystalline phase. Since the fluidity of the liquid crystalline PMA matrix should be dramatically increased in the isotropic phase, the azobenzene units would be rearranged to form the H-aggregated and homeotropic alignment as the most stable state. Similarly, considerable hypsochromic shift (9 nm) and hypochromic effect (55%) were also observed in the $\pi-\pi^*$ long axis transition of the stilbene unit after annealing of $\mathbf{bCC_{45}}$ films. On the contrary, the $\pi-\pi^*$ short axis transition seems a noticeable hypochromic effect around 250 nm, which cannot be discussed further due to the most serious scattering tail superimposed in the UV region in all four block copolymer films. The higher energy absorption of two $\pi-\pi^*$ long axis transitions of the benzylideneaniline unit in $\mathbf{bCN_{53}}$ thin film was blue-shifted by 5 nm and decreased 67%, while the lower energy one as a shoulder was buried in the longer one. These considerable hypsochromic shift and hypochromic effect observed commonly in the spectra of $\mathbf{bNN_{56}}$, $\mathbf{bCN_{53}}$, and $\mathbf{bCC_{45}}$ thin films implies the formation of the strong H-aggregation and homeotropic alignment of the mesogen moieties in the PMA matrix.

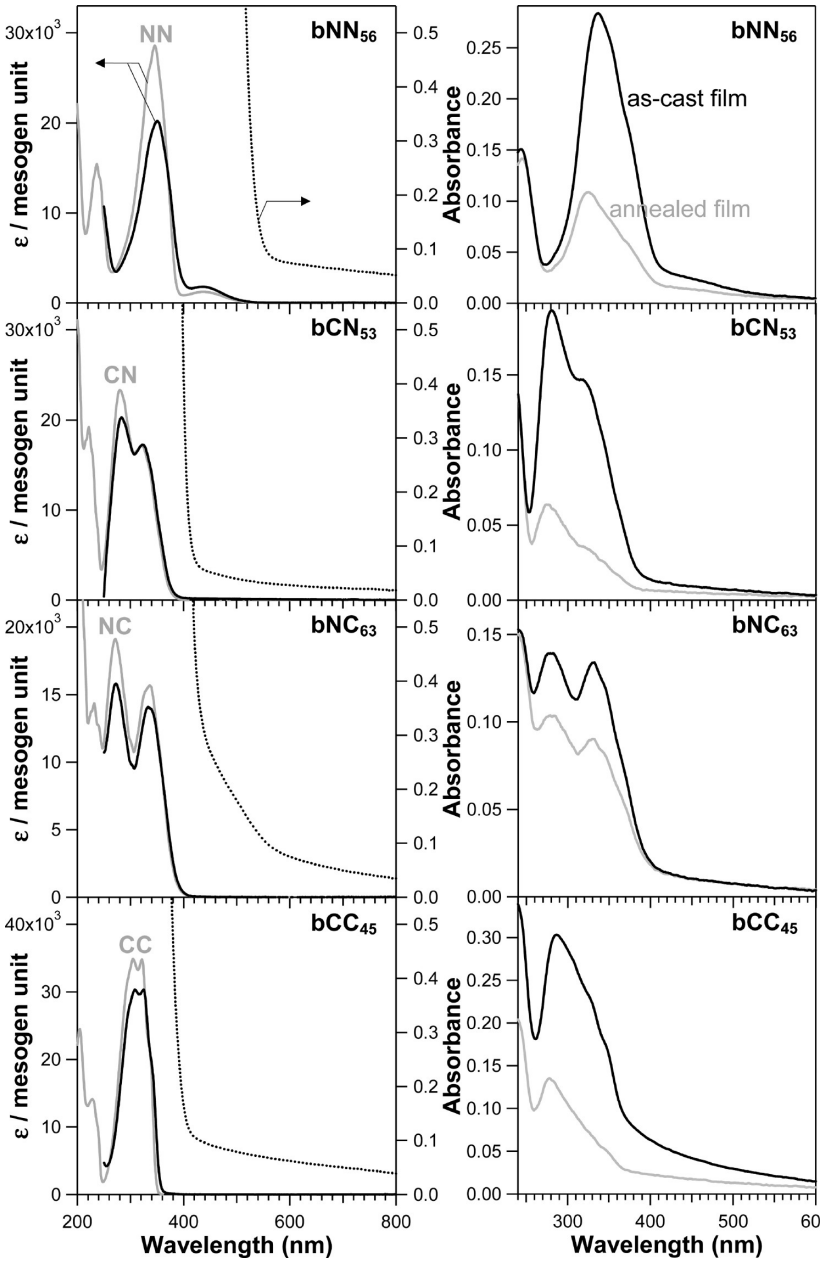

Figure 11. UV−vis spectra of amphiphilic diblock copolymers. Left traces: spectra in chloroform solution at the concentration of $(3.3-3.6) \times 10^{-5}$ M (black lines) and $(5.1-5.5) \times 10^{-2}$ M (dotted black lines) per mesogen chromophore, together with those of corresponding model compounds in hexane solution at $(4.0-4.9) \times 10^{-5}$ M (gray lines). The right traces: spectra of the as-cast (black lines) and annealed films (gray lines). The films were fabricated by spin-coating from 2 wt % chloroform solution onto quartz glass. The films of **bNN$_{56}$**, **bCN$_{53}$**, and **bNC$_{63}$** were annealed at 140 °C for 24 h, and that of **bCC$_{45}$** was annealed at 190 °C for 2 h.

The mesogens of **bNN$_{56}$**, **bCN$_{53}$**, and **bCC$_{45}$** should be arranged almost perpendicularly against the film surface, judging from the H-aggregation observed on annealing. Since the PEO cylindrical domains also aligned perpendicularly to the film surface, as shown in the TEM images, the mesogens were arranged parallel to the long axis of the PEO cylinders. As we reported previously,[85] an AFM observation of the cross section of the cleaved spin-cast film of **bNN$_{56}$** on the silicon wafer figured out perpendicularly oriented PEO cylindrical domains with 430 of aspect ratio, which fully penetrated across the film thickness. Assuming that the PMA side chains are extended and packed densely in the glass state at room temperature, the smectic layers should be tilted against the phase segregated interface since the liquid crystalline phase of **bNN$_{56}$** was assigned as a tilted smectic phase. More obviously in the case of 1.0 μm thick film, a bent structure along the PEO cylinders was observed on the cross-sectional surface, which would be originated from a kind of conflict between the perpendicularly oriented PEO cylinders and a tilting structure of the mesogens. On the other hand, **bCN$_{53}$** and **bCC$_{45}$** exhibit the SmA phase, and thus such a conflict may not occur. Their mesogens could be aligned parallel to the cyrinders, and the smectic layers might be perpendicularly arranged against the phase-segregated interface.

Quite a difference was found in two $\pi-\pi^*$ long axis transitions of the benzylideneaniline unit in **bNC$_{63}$** thin film. The 270 and

337 nm absorption maxima in chloroform solution were red-shifted by 9 nm and blue-shifted by 6 nm in as-cast film, respectively. Both hypochromic effects (25% and 33%) after annealing are exclusively smaller than those in **bNN$_{56}$**, **bCN$_{53}$**, and **bCC$_{45}$**, implying that homeotropic alignment of the benzylideneanilene chromophore in **bNC$_{63}$** thin film should be insufficient upon annealing. The mesogen units in the smectic layered structure, which the X-ray measurement indicated in the **bNC$_{63}$** thin film, should be less ordered compared with the others. It can be concluded that such less ordered mesogen units in **bNC$_{63}$** should cause less oriented cylinder structure. Furthermore, no blue shift of the absorption maxima implies little H-aggregation after annealing, and in other words, stacking interaction between the benzylidenaniline chromophores in **bNC$_{63}$** thin film could be so weak compared with the other block copolymers. The authors have concluded here that such H-aggregation of the mesogen chromophores in smectic layered structure should play an important role in the normally oriented and highly ordered hexagonal cylinder structures on various kinds of non-pretreated substrates with high aspect ratio up to 430, which has scarcely been achieved in conventional block copolymers such as PS-*b*-PMMA.

The strong stacking interactions between the mesogens enough to show a H-aggregation should be indispensable to make a highly ordered cylindrical nanostructure as shown in the thin films of **bNN$_{56}$**, **bCN$_{53}$**, and **bCC$_{45}$**. These nanostructures might be formed through the cooling process on annealing. As shown by temperature-dependent SAXS measurements, an order-to-order transition should occur at the isotropic-to-smectic liquid crystalline phase transition temperature in the case of the copolymers having relatively shorter PMA segments. This fact also strongly indicates that the anisotropic arrangement of liquid crystalline segments should determine not only the anisotropy of nanostructure but also the microphase symmetry. As the temperature of the film surface should be slightly lower than that inside the film, the liquid crystalline transition might occur at the surface at first and then propagate into the film, which looks like a growth of crystals. In this context, the domain size of liquid crystalline phase should be a key factor to determine the quality of ordering cylindrical nanostructure.

CONCLUSIONS

A new series of amphiphilic liquid crystalline diblock copolymers consisting PEO and PMA with azobenzene derivatives as the mesogen cores in the side chain were synthesized with narrow polydispersities by the ATRP method. While the azobenzene-tethered side-chain liquid crystalline polymers exhibited SmC phase at room temperature, the other polymers having benzylideneaniline and stilbene in the mesogens instead of azobenzene gave the thermal properties assigned as SmA phase. Irrelevant of the mesogen structure, hexagonally arranged PEO cylindrical domain was assigned as a common microphase-separated nanostructure by SAXS measurement in the annealed bulk pellet of each block copolymer. Moreover, perpendicular orientation of the PEO cylindrical domains was verified by TEM and AFM observations as a common nanostructure characteristic of all the block copolymer thin films except **bNC**s, of which hexagonal cylinder nanostructure seems less ordered with respect to size and orientation of well-ordered domain structures, i.e., limited as short-range ordering. Such specificity on microphase-separated nanostructure of **bNC**s has not yet been fully figured out in this study by DSC, WAXS, and POM measurements. Hypsochromic shifts and large hypochromic effects observed after annealing in the UV−vis spectra of **bNN**, **bCN**, and **bCC** films suggest the formation of the strongly H-aggregated and homeotropic alignment of mesogens in the liquid crystalline PMA matrix, which should play a key role to regulate the direction of propagation of cylindrical PEO domain upon annealing and to form such a highly ordered nanostructure. Further detailed analysis should be required.

As we demonstrated in this paper, the combination of the side-chain liquid crystalline copolymer and the strong segregation as amphiphilicity is a powerful method for giving an excellent regularity and a high anisotropy to the phase-segregated nanostructure. Together with the direct observations of the cross-sectional image of nanostructures by AFM, further investigations upon the mechanism of nanostructure formation as well as the exact orientation of liquid crystalline mesogen units by using a grazing incidence small-angle X-ray scattering (GI-SAXS) and/or a temperature-dependent AFM measurement will be reported in another paper.

EXPERIMENTAL SECTION

General. ^{1}H and ^{13}C NMR spectra were obtained on JEOL EX270, EX400, and LA500 spectrometers in chloroform-*d*. Infrared spectra were obtained on a JASCO FT/IR-600 plus instrument. Mass spectra were measured on a JEOL JMS-700 in FAB mode using *m*-nitrobenzyl alcohol (NBA) as a matrix and/or on a Bruker microTOF focus in ESI mode using methanol solution. Molecular weights of polymers were determined by gel permeation chromatography (GPC) eluted by THF on a TSK-gel H$_{XL}$-M column (Tosoh) in reference of a series of standard polystyrene using a JASCO liquid chromatography system composed of a PU-980 HPLC pump and an 860-CO column oven (operated at 35 °C) equipped with an ERMA ERC-8710 UV and a Shodex RI-101 RI detector. The number-averaged molecular weight (M_N) and the weight-averaged molecular weight (M_W) were calculated by using polystyrenes (Tosoh) as standards.

Thermal analyses were conducted under N_2 flow on an SII Extra 6000 DSC system (Seiko Instruments Inc.) at a scanning rate of ±10 °C/min. Temperature-dependent polarized optical microscopic (POM) observation was conducted under Ar flow by using an Olympus BX51/BX52 microscope fitted with a Mettler Toled FP900 thermo-control system. Temperature-dependent wide-angle X-ray diffraction (WAXD) was measured with a Mac Science M21X-SRA using Cu Kα source, and small-angle X-ray scattering (SAXS) measurements were carried out at the beamline 10C in Photon Factory, High Energy Accelerator Research Organization (Tsukuba, Japan), by using a one-dimensional position-sensitive proportional counter (Rigaku) as a detector.

TEM images were obtained by using a Hitachi H-7000 electron microscope at an acceleration voltage of 200 kV. The sample for observation were prepared subject to the following procedure. The spin-coated films from the 2 wt % toluene solutions of the block copolymers on the fresh surface of mica substrates were annealed above the isotropic transition temperature under vacuum without any precise control of the heating and cooling rate. The obtained thin films were easily peeled from the substrates by soaked in water, then transferred onto copper TEM grids, and exposed on RuO_4 vapor at room temperature for 2 min to selectively stain the PEO domains.

AFM measurements were made by a Multi Mode scanning probe microscope, Nanoscope IV (Digital Instrument), equipped with Tapping Mode silicon cantilevers (Nano Devices, with a normal frequency of 300 kHz). The samples for observation were prepared subject to the following procedure. The 0.5−4.0 wt % toluene or chloroform solutions of the block copolymers were spin- or bar-coated on (100) silicon wafer (Fujimi Fine Technology, Inc., Japan) substrates, which

had been cleaned with acetone by ultrasonication for 10 min. The films on the substrates were annealed above the isotropic transition temperature under vacuum without any precise control of the heating and cooling rate.

Materials. Dichloromethane was fractionally distilled from calcium hydride. Anisole was fractionally distilled from melting sodium with benzophenone. The other chemicals were commercial products used as received.

While the synthesis of the monomer **mNN** was described in our previous report,[84] those of the other monomers (**mCN**, **mNC**, and **mCC**) and the corresponding model compounds (**NN**, **CN**, **NC**, and **CC**) are described in the Supporting Information. The initiators, benzyl 2-bromo-2-methylpropionate (BzO-BMP) and α-methoxypoly(ethylene oxide)−ω-(2-bromo-2-methylpropionate) (PEO-BMP), were synthesized by esterification of benzyl alcohol (Wako) and poly(ethylene oxide) monomethyl ether (M_W = 5000, NOF), respectively, with 2-bromo-2-methylpropionyl bromide (TCI) according to a similar procedure as reported previously.[84]

Polymerization. All the block copolymers **bNN**s, **bCN**s, **bNC**s, and **bCC**s were synthesized via ATRP according to a typical procedure as follows. A mixture of copper(I) chloride (17 mg, 172 μmol) and 1,1,4,7,10,10-hexamethylenetetramine (HMTETA, 50 μL, 184 μmol) in anisole (1 mL) was added to the anisole (4 mL) solution containing PEO-BMP (87 mg, 17 μmol) and monomer **mCN** (492 mg, 1 mmol) under an argon atmosphere. The reaction mixture was sealed in the tube and then heated at 80 °C for 22 h. The reaction mixture was passed through an activated basic alumina (Merck) column using chloroform as eluent to remove the copper complex. After the solvent was removed under reduced pressure, the residue was taken for ^{1}H NMR measurement in order to determine the conversion.[99] The residual solid was washed with hot hexane repeatedly to remove the remaining monomer. The residue was then dissolved in a minimum amount of chloroform and reprecipitated in methanol to give $\mathbf{bCN}_{53}$ as colorless powder (265 mg, 46%), which was served as an isolated polymer sample for characterization. All the homopolymers **hNN**s, **hCN**s, **hNC**s, and **hCC**s were prepared according to the same procedure by using BzO-BMP as an initiator. The polymerization degrees (DPs) of homo- and copolymers were determined from the ratio of the peak area corresponding to the four methylene protons at the both ends of the undecyl linker in each monomer unit against that to the two α-methylene proton of benzyl unit and that to the four methylene units in each monomer unit of poly(ethylene oxide), respectively. The detailed polymerization condition and properties of all homo- and copolymers are described in the Supporting Information.

■ ASSOCIATED CONTENT

Ⓢ Supporting Information. Detailed discussion about the "intralayer" regularity of liquid crystalline mesogens; procedures for the preparation of the monomers (**mNN**, **mCN**, **mNC**, and **mCC**), their model compounds (**NN**, **CN**, **NC**, and **CC**), initiators, and polymers; DSC curves and SAXS profiles of diblock copolymers. This material is available free of charge via the Internet at http://pubs.acs.org.

■ AUTHOR INFORMATION

Corresponding Author

*Tel +81-75-724-7768, e-mail sada@kit.ac.jp (S.A.). Tel +81-45-924-5233, Fax +81-45-924-5277, e-mail iyoda.t.aa@m.titech.ac.jp (T.I.).

■ ACKNOWLEDGMENT

This work was partially supported by Grant-in-Aid for Scientific Research (S) (No. 90168534) and (B) (No. 20310056). The poly(ethylene oxide) used for copolymer synthesis was kindly provided by NOF Corporation. We thank to Dr. Y. Tian for providing the preliminary concept for molecular design. We also thank Dr. K. Kamata at Tokyo Institute of Technology for her discussions and assistance during experiments.

■ REFERENCES

(1) Aggarwal, S. L. *Polymer* **1976**, *17*, 938.
(2) Bates, F. S.; Schulz, M. F.; Khandpur, A. K.; Förster, S.; Rosedale, J. H.; Almdal, K.; Mortensen, K. *Faraday Discuss.* **1994**, *98*, 7.
(3) Khandpur, A. K.; Foerster, S.; Bates, F. S.; Hamley, I. W.; Ryan, A. J.; Bras, W.; Almdal, K.; Mortensen, K. *Macromolecules* **1995**, *28*, 8796.
(4) Matsen, M. W.; Bates, F. S. *Macromolecules* **1996**, *29*, 1091.
(5) Grubbs, R. H.; Tumas, W. *Science* **1989**, *243*, 907.
(6) *Living and Controlled Polymerization: Synthesis, Characterization and Properties of the Respective Polymers and Copolymers*; Jagur-Grodzinski, J., Ed.; Nova Science Publishers: New York, 2006.
(7) *Controlled Radical Polymerization*; Matyjaszewski, K., Ed.; American Chemical Society: Washington, DC, 1998.
(8) *Controlled/Living Radical Polymerization. Progress in ATRP, NMP, and RAFT*; Matyjaszewski, K., Ed.; American Chemical Society: Washington, DC, 2000.
(9) *Advances in Controlled/Living Radical Polymerization*; Matyjaszewski, K., Ed.; American Chemical Society: Washington, DC, 2003.
(10) *Controlled/Living Radical Polymerization from Synthesis to Materials*; Matyjaszewski, K., Ed.; American Chemical Society: Washington, DC, 2006.
(11) Odian, G. *Principles of Polymerization*, 4th ed.; Wiley: New York, 2004.
(12) Schrock, R. R. *Acc. Chem. Res.* **1990**, *23*, 158.
(13) Webster, O. W. *Science* **1991**, *251*, 887.
(14) *Processing, Structure, and Properties of Block Copolymers*; Folkes, M. J., Ed.; Elsevier Applied Science Publishers: London, 1985.
(15) Foerster, S.; Khandpur, A. K.; Zhao, J.; Bates, F. S.; Hamley, I. W.; Ryan, A. J.; Bras, W. *Macromolecules* **1994**, *27*, 6922.
(16) Hasegawa, H.; Tanaka, H.; Yamasaki, K.; Hashimoto, T. *Macromolecules* **1987**, *20*, 1651.
(17) Spontak, R. J.; Smith, S. D.; Ashraf, A. *Macromolecules* **1993**, *26*, 956.
(18) Thomas, E. L.; Alward, D. B.; Kinning, D. J.; Martin, D. C.; Handlin, D. L.; Fetters, L. J. *Macromolecules* **1986**, *19*, 2197.
(19) Lazzari, M.; Lopez-Quintela, M. A. *Adv. Mater.* **2003**, *15*, 1583.
(20) Park, C.; Yoon, J.; Thomas, E. L. *Polymer* **2003**, *44*, 6725.
(21) Segalman, R. A. *Mater. Sci. Eng., R* **2005**, *48*, 191.
(22) Timothy, P. L. *Macromol. Chem. Phys.* **2003**, *204*, 265.
(23) Templin, M.; Franck, A.; Du Chesne, A.; Leist, H.; Zhang, Y.; Ulrich, R.; Schadler, V.; Wiesner, U. *Science* **1997**, *278*, 1795.
(24) Ikkala, O.; ten Brinke, G. *Science* **2002**, *295*, 2407.
(25) Kato, T. *Science* **2002**, *295*, 2414.
(26) Li, J.; Kamata, K.; Komura, M.; Yamada, T.; Yoshida, H.; Iyoda, T. *Macromolecules* **2007**, *40*, 8125.
(27) Harrison, C.; Park, M.; Chaikin, P. M.; Register, R. A.; Adamson, D. H. *J. Vac. Sci. Technol., B: Microelectron. Nanometer Struct.—Process., Meas., Phenom.* **1998**, *16*, 544.
(28) Haupt, M.; Miller, S.; Ladenburger, A.; Sauer, R.; Thonke, K.; Spatz, J. P.; Riethmuller, S.; Moller, M.; Banhart, F. *J. Appl. Phys.* **2002**, *91*, 6057.
(29) Spätz, J. P.; Herzog, T.; Mössmer, S.; Ziemann, P.; Möller, M. *Adv. Mater.* **1999**, *11*, 149.
(30) Boontongkong, Y.; Cohen, R. E. *Macromolecules* **2002**, *35*, 3647.
(31) Fahmi, A. W.; Braun, H. G.; Stamm, M. *Adv. Mater.* **2003**, *15*, 1201.
(32) Haryono, A.; Binder, W. H. *Small* **2006**, *2*, 600.
(33) Kim, D. H.; Kim, S. H.; Lavery, K.; Russell, T. P. *Nano Lett.* **2004**, *4*, 1841.

(34) Li, J.; Kamata, K.; Watanabe, S.; Iyoda, T. *Adv. Mater.* **2007**, *19*, 1267.
(35) Lopes, W. A.; Jaeger, H. M. *Nature* **2001**, *414*, 735.
(36) Ribbe, A. E.; Okumura, A.; Matsushige, K.; Hashimoto, T. *Macromolecules* **2001**, *34*, 8239.
(37) Yeh, S. W.; Wei, K. H.; Sun, Y. S.; Jeng, U. S.; Liang, K. S. *Macromolecules* **2003**, *36*, 7903.
(38) *Liquid Crystal Polymers: From Structures to Applications*; Collyer, A. A., Ed.; Elsevier Applied Science: London, 1992.
(39) *Liquid Crystalline Polymers*, 2nd ed.; Donald, A. M., Windle, A. H., Hanna, S., Eds.; Cambridge University Press: Cambridge, 2006.
(40) *Liquid Crystal Polymers*; Gordon, M.; Plate, N. A., Eds.; Springer-Verlag: Berlin, 1984; Vols. 1−3.
(41) *Liquid-Crystalline Polymer Systems: Technological Advances*; Isayev, A. I., Kyu, T., Cheng, S. Z. D., Eds.; American Chemical Society: Washington, DC, 1996.
(42) *Liquid-Crystalline Polymers*; Weiss, R. A., Ober, C. K., Eds.; American Chemical Society: Washington, DC, 1990.
(43) Lambert, J. M.; Yilgor, E.; Yilgor, I.; Wilkes, G. L.; McGrath, J. E. *Polym. Prepr.* **1985**, *26*, 275.
(44) Fischer, H.; Poser, S. *Acta Polym.* **1996**, *47*, 413.
(45) Mao, G.; Ober, C. K. *Acta Polym.* **1997**, *48*, 405.
(46) Angeloni, A. S.; Bignozzi, M. C.; Laus, M.; Chiellini, E.; Galli, G. *Polym. Bull.* **1993**, *31*, 387.
(47) Auman, B. C.; Percec, V. *Polymer* **1988**, *29*, 938.
(48) Radzilowski, L. H.; Stupp, S. I. *Macromolecules* **1994**, *27*, 7747.
(49) Sonpatki, M. M.; Ravindranath, K.; Ponrathnam, S. *Polymer* **1995**, *36*, 3127.
(50) Figueiredo, P.; Gronski, W.; Bach, M. *Macromol. Rapid Commun.* **2002**, *23*, 38.
(51) Gabert, A. J.; Verploegen, E.; Hammond, P. T.; Schrock, R. R. *Macromolecules* **2006**, *39*, 3993.
(52) Koltzenburg, S.; Ungerank, M.; Stelzer, F.; Nuyken, O. *Macromol. Chem. Phys.* **1999**, *200*, 814.
(53) Komiya, Z.; Schrock, R. R. *Macromolecules* **1993**, *26*, 1387.
(54) Laus, M.; Bignozzi, M. C.; Fagnani, M.; Angeloni, A. S.; Galli, G.; Chiellini, E.; Francescangeli, O. *Macromolecules* **1996**, *29*, 5111.
(55) Poster, S.; Arnold, M.; Fischer, H. *Eur. Polym. J.* **1996**, *32*, 1169.
(56) Robert Bohnert, H. F. *Macromol. Chem. Phys.* **1994**, *195*, 689.
(57) Singh, R.; Verploegen, E.; Hammond, P. T.; Schrock, R. R. *Macromolecules* **2006**, *39*, 8241.
(58) Walther, M.; Faulhammer, H.; Finkelmann, H. *Macromol. Chem. Phys.* **1998**, *199*, 223.
(59) Wewerka, K.; Wewerka, A.; Stelzer, F.; Gallot, B.; Andruzzi, L.; Galli, G. *Macromol. Rapid Commun.* **2003**, *24*, 906.
(60) Yamada, M.; Hirao, A.; Nakahama, S.; Iguchi, T.; Watanabe, J. *Macromolecules* **1995**, *28*, 50.
(61) Zheng, W. Y.; Hammond, P. T. *Macromolecules* **1998**, *31*, 711.
(62) Poser, S.; Fischer, H.; Arnold, M. *Prog. Polym. Sci.* **1998**, *23*, 1337.
(63) Fischer, H.; Poser, S.; Arnold, M.; Frank, W. *Macromolecules* **1994**, *27*, 7133.
(64) Poser, S.; Fischer, H.; Arnold, M. *J. Polym. Sci., Part A: Polym. Chem.* **1996**, *34*, 1733.
(65) Mao, G.; Wang, J.; Clingman, S. R.; Ober, C. K.; Chen, J. T.; Thomas, E. L. *Macromolecules* **1997**, *30*, 2556.
(66) Mao, G.; Wang, J.; Ober, C. K.; Brehmer, M.; O'Rourke, M. J.; Thomas, E. L. *Chem. Mater.* **1998**, *10*, 1538.
(67) Anthamatten, M.; Zheng, W. Y.; Hammond, P. T. *Macromolecules* **1999**, *32*, 4838.
(68) Ansari, I. A.; Castelletto, V.; Mykhaylyk, T.; Hamley, I. W.; Lu, Z. B.; Itoh, T.; Imrie, C. T. *Macromolecules* **2003**, *36*, 8898.
(69) Al-Hussein, M.; Serero, Y.; Konovalov, O.; Mourran, A.; Moller, M.; deJeu, W. H. *Macromolecules* **2005**, *38*, 9610.
(70) Hamley, I. W.; Castelletto, V.; Parras, P.; Lu, Z. B.; Imrie, C. T.; Itoh, T. *Soft Matter* **2005**, *1*, 355.
(71) Verploegen, E.; McAfee, L. C.; Tian, L.; Verploegen, D.; Hammond, P. T. *Macromolecules* **2007**, *40*, 777.
(72) Zaschke, B.; Frank, W.; Fischer, H.; Schmutzler, K.; Arnold, M. *Polym. Bull.* **1991**, *27*, 1.
(73) Wong, G. C. L.; Commandeur, J.; Fischer, H.; de Jeu, W. H. *Phys. Rev. Lett.* **1996**, *77*, 5221.
(74) Sentenac, D.; Demirel, A. L.; Lub, J.; De Jeu, W. H. *Macromolecules* **1999**, *32*, 3235.
(75) Anthamatten, M.; Hammond, P. T. *Macromolecules* **1999**, *32*, 8066.
(76) Schneider, A.; Zanna, J.-J.; Yamada, M.; Finkelmann, H.; Thomann, R. *Macromolecules* **2000**, *33*, 649.
(77) Forcén, P.; Oriol, L.; Sánchez, C.; Alcalá, R.; Hvilsted, S.; Jankova, K.; Loos, J. *J. Polym. Sci., Part A: Polym. Chem.* **2007**, *45*, 1899.
(78) Deng, W.; Albouy, P.-A.; Lacaze, E.; Keller, P.; Wang, X.; Li, M.-H. *Macromolecules* **2008**, *41*, 2459.
(79) Ding, L.; Mao, H.; Xu, J.; He, J.; Ding, X.; Russell, T. P.; Robello, D. R.; Mis, M. *Macromolecules* **2008**, *41*, 1897.
(80) Anthamatten, M.; Wu, J.-S.; Hammond, P. T. *Macromolecules* **2001**, *34*, 8574.
(81) Tenneti, K. K.; Chen, X.; Li, C. Y.; Tu, Y.; Wan, X.; Zhou, Q.-F.; Sics, I.; Hsiao, B. S. *J. Am. Chem. Soc.* **2005**, *127*, 15481.
(82) Walther, M.; Finkelmann, H. *Prog. Polym. Sci.* **1996**, *21*, 951.
(83) Verploegen, E.; Zhang, T.; Jung, Y. S.; Ross, C.; Hammond, P. T. *Nano Lett.* **2008**, *8*, 3434.
(84) Tian, Y.; Watanabe, K.; Kong, X.; Abe, J.; Iyoda, T. *Macromolecules* **2002**, *35*, 3739.
(85) Komura, M.; Iyoda, T. *Macromolecules* **2007**, *40*, 4106.
(86) Yamamoto, T.; Kimura, T.; Komura, M.; Suzuki, Y.; Iyoda, T.; Asaoka, S.; Nakanishi, H. *Adv. Funct. Mater.* **2011**, *21*, 918.
(87) Watanabe, S.; Fujiwara, R.; Hada, M.; Okazaki, Y.; Iyoda, T. *Angew. Chem., Int. Ed.* **2007**, *46*, 1120.
(88) Watanabe, R.; Kamata, K.; Iyoda, T. *J. Mater. Chem.* **2008**, *18*, 5482.
(89) Watanabe, R.; Kamata, K.; Iyoda, T. *Jpn. J. Appl. Phys., Part 1* **2008**, *47*, 5039.
(90) Watanabe, R.; Ito, K.; Iyoda, T.; Sakaguchi, H. *Jpn. J. Appl. Phys., Part 2* **2009**, *48*, 06FE08.
(91) Chen, A.; Komura, M.; Kamata, K.; Iyoda, T. *Adv. Mater.* **2008**, *20*, 763.
(92) Suzuki, S.; Kamata, K.; Yamauchi, H.; Iyoda, T. *Chem. Lett.* **2007**, *36*, 978.
(93) Yu, H.; Li, J.; Ikeda, T.; Iyoda, T. *Adv. Mater.* **2006**, *18*, 2213.
(94) Weinstein, J.; McIninch, E. *J. Am. Chem. Soc.* **1960**, *82*, 6064.
(95) Scherrer, P. *Nachr. Ges. Wiss. Göttingen* **1918**, 98.
(96) Yoon, J.; Jung, S. Y.; Ahn, B.; Heo, K.; Jin, S.; Iyoda, T.; Yoshida, H.; Ree, M. *J. Phys. Chem. B* **2008**, *112*, 8486.
(97) Morikawa, Y.; Kondo, T.; Nagano, S.; Seki, T. *Chem. Mater.* **2007**, *19*, 1540.
(98) Morikawa, Y.; Nagano, S.; Watanabe, K.; Kamata, K.; Iyoda, T.; Seki, T. *Adv. Mater.* **2006**, *18*, 883.
(99) Conversions were determined from the ratio of peak areas corresponding to the two vinyl protons of methacrylate against that to the eight protons on aromatic ring in ^{1}H NMR spectra. Althogh the aromatic protons were unaffected in the course of polymerization, the vinyl protons were converted to methylene protons to form the polymer main chain.